RSC Advances

Journal Name RSC Advances Dynamic Article Links ►

Cite this: DOI: 10.1039/c0xx00000x

www.rsc.org/xxxxxx

ARTICLE TYPE

Studies on salophen anchored micro/meso porous activated carbon fibres for the removal and recovery of Uranium

Shruti Mishra[a,b], Jaya Dwivedi[b], Amar Kumar[c] and Nalini Sankararamakrishnan[a*]

Received (in XXX, XXX) Xth XXXXXXXXX 20XX, Accepted Xth XXXXXXXXX 20XX
DOI: 10.1039/b000000x

Abstract

Stringent environmental regulations emphasizes on the removal of Uranium from aqueous systems. Activated carbon fibers (ACF) was functionalized by oxidation (ACF-OX) and salophen ligand (ACF-Sal) and evaluated for the removal of Uranium. The prepared sorbents were characterized by various techniques like Scanning Electron Microscopy (SEM), Energy Dispersive X-ray (EDAX), Fourier Transform Infra Red (FTIR) and Brunauer, Emmett, and Teller (BET) surface area analyzer and X-ray Photoelectron spectroscopy (XPS). Anchoring of salophen ligand onto ACF surface was evident from FTIR and XPS studies. The adsorption properties of UO_2^{2+} as a function of pH, and contact time were characterized by Inductively coupled Mass Spectrometer (ICPMS). The adsorption kinetics fitted the Pseudo Second Order Kinetics and equilibrium reached within 180 minutes. The experimental data were modelled with Langmuir and Freundlich, isotherms and various isotherm parameters were evaluated. Maximum adsorption capacity of U(VI) at pH 6 for ACF, ACF-OX and ACF-Sal were found to be 22.2, 50.0 and 142.8 mg/g respectively. Thermodynamic studies revealed the spontaneity of the reaction and influence of other cations and anions on sorption behaviour of uranium was also carried out. Studies have been conducted to demonstrate the recyclability of the sorbent for five consecutive sorption desorption cycles. Using FTIR and XPS studies a suitable mechanism for uranium sorption has also been postulated.

Key words: Uranium, Adsorption, Activated Carbon Fibres, Salophen

1. Introduction

Uranium is the second heaviest naturally occurring radioactive element. Uranium is the basic energy element of the present Indian nuclear power programme. It starts as a source of the fuel cycle and finally ends up as a waste component. Uranium is well known nephrotoxic heavy metal. It is reported that an exposure of 0.1 mg/Kg of body weight of natural U results in transient chemical damage to kidneys[1]. The maximum contaminant level of U(VI) in water by Environment Protection Agency (EPA) is 30 µg/L whereas the World Health Organization's guideline value is set at 50 µg/L[2]. According to Atomic Energy Research Board (AERB) of India the maximum allowable concentration of U(VI) in water bodies is 60 µg/L. In aquatic environment uranium predominantly exists in its hexavalent oxidation state e.g. UO_2^{2+}. These hexavalent uranyl ions are highly mobile and migrate as stable uranyl carbonate complexes under near surface conditions[3]. Cost effective remediation technology is required to tackle removal of uranium from large volumes of wastewaters. Several methods are utilized to remove uranium from wastewater and process effluents. These include ion exchange, reduction, reduction followed by chemical precipitation, electrochemical precipitation, membrane separation, solvent extraction, biosorption, adsorption etc. Among the various removal technologies for U(VI) reported, adsorption is the most versatile technique owing to its ease of operation, low waste generation and considerably low recurring cost. Removal of U(VI) by various adsorbents have been adequately reviewed[4,5]. Carbon based sorption materials offer various advantages including higher radiation and thermal resistance than commonly used organic exchange resins and improved chemical stability than widely used inorganic sorbents in strongly acidic solutions in the majority of nuclear wastewaters[4]. Carbonaceous materials including activated carbon[6,7], activated carbon fibres, carbon nanotubes[8-10] and mesoporous carbon[11] have been reported in the applications of U(VI) sorption. To improve the selectivity and sorption capacity towards targeted metal ions functionalization with specific ligands are generally resorted[4]. Among these carbonaceous materials, activated carbon fibres (ACF) are unique owing to large porous surface area, controllable pore structure, thermo-stability and low acid/base reactivity. Further, ACFs are microporous materials possessing high surface area (~ 1200 – 1800 m^2/g), which is a prime factor for an adsorbent. In ACF, micropores which are responsible for adsorption are connected to the external surface directly by narrow diameter fibre ((10 – 20 µm). Thus diffusion length is small and therefore this result in negligible mass transfer coefficient and the removal rate of pollutants is adsorption controlled[12]. ACFs have been found useful for the removal of variety of pollutants like Cd(II) and Pb(II)[12-14], Ni(II) and Zn(II)[15-17], SO_2, NO and CO_2[18], 2-chloroethanol[19] etc. Jung et al.[20] have reported the electrosorption of uranium (U(VI)) ions onto a porous ACF. However, there are seldom any reports in the literature on the use of functionalized ACFs towards U(VI) removal. It is well known that salophen is a tetradentate ligand that can easily combine with uranyl cation to form stable uranyl-salophen complex[21,22] and has been found useful for the determination of trace U(VI). Thus this work pertains to the development of functionalized activated carbon fibres by oxidation (ACF-OX) and grafting of salophen ligand (ACF-Sal) and its applicability to U(VI) removal. Systematic structural characterization of the functioalized sorbents namely ACF-OX and ACF-Sal were performed using various techniques and optimization of reaction parameters including pH, reaction time, were carried out. Isotherm, thermodynamic and kinetic models were evaluated and a suitable mechanism for the adsorption of U(VI) using FTIR and XPS has also been postulated.

2. Materials and Methods

All chemicals, sodium hydroxide (NaOH), nitric acid (HNO_3), uranyl(VI) nitrate ($UO_2(NO_3)_2.6H_2O$), and other reagents and solvents (ethanol, acetone) used in this study were analytical grade and all solutions were prepared using Milli-Q purified water (resistivity > 18.2 MΩ cm). 4-hydroxysalicylaldehyde , thionyl chloride and 1,2 diaminoethane were acquired from Sigma Aldrich chemicals. Activated carbon fibres were purchased from Nippon Kynol In. (Osaka Japan).

2.1 Preparation of ACF-OX

Around 1 g of ACF samples were treated with 20 ml of 1:1 mixture of Conc. HNO_3 and water and heated at 60˚C for 30 min. followed by thorough washing with distilled water and dried in an oven for 12 h at 120˚C.

2.2 Preparation of Salophen ligand

The stoichiometric amount of 4-Methoxysalicylaldehyde (0.02 mol, 2.76 g) in dissolved methanol (25 ml) is added drop- by-drop to 1,2-diaminoethane solution (0.01 mol, 0.60 g) in 25 ml methanol. The contents were refluxed for 4 h and a bright yellow precipitate of symmetrical Schiff-base ligand; $H_2[(OH)_2$-salen]; was obtained.

2.3 Preparation of ACF-Sal:

Initially chlorinated ACFs were prepared. Around 100 mg of ACFs were suspended in a solution of $SOCl_2$ (25 ml) and DMF (1 ml). The suspension was stirred at 65 ºC for 24 h. The solid was then separated by filtration and washed with anhydrous THF, and dried in vacuum.To a solution of Salophen (100 mg) in degassed $CHCl_3$ (8 ml), chlorinated ACFs were added (50 mg) and the suspension was stirred for 20 h under N_2 atmosphere at 70º C. The solid was then separated by filtration and exhaustively washed with THF and CH_2Cl_2 and dried in vacuum.
The schematic representation of the preparation of ACF-OX and ACF-Sal is shown in scheme 1[23].

2.4 Batch Studies

Adsorption experiments were carried out by batch technique. About 0.05 g of adsorbent were placed in a beaker containing 20 mL of 0.1 to 500 mgL^{-1} of U(VI) solution for ACF and ACF-OX and 0.1 to 1000 mgL^{-1}. for ACF-Sal. The pH of the solution was adjusted to 6.0 by adding 10% sodium hydroxide or 10% sulphuric acid solutions. The suspension was stirred for 3 h at an agitation speed of 110 rpm. At the end of the equilibrium time, the content was separated by filtration with 0.22µm pore size filter paper and U(VI) in solution was analyzed by inductive coupled plasma-mass spectrometry (ICP-MS) (Thermo Scientific, XSERIES 2). All the experiments were repeated twice. The amount of the U(VI) adsorbed (mg) per unit mass of sorbent (g), *qe*, was obtained by mass balance using the following equation:

$$qe = \frac{(c_i - c_e)}{m} \times V \quad (1)$$

Where *Ci* and *Ce* are initial and equilibrium concentrations of the U(VI) (mg L^{-1}), *m* is dry mass of sorbent (g) and *V* is the volume of the solution (L). Kinetic experiments were conducted by equilibrating 20 mL of 100 mg L^{-1} of U(VI) at a dose rate of 5.0 g L^{-1} and pH was maintained at 6.0 during equilibration. The amount of uranium adsorbed was monitored at regular time intervals. The effect of competing cations and anions were examined by maintaining the initial concentration of uranium at 100 mg L^{-1}. Using the same conditions mentioned above, thermodynamic studies were carried out by equilibrating the solutions for 3 h at three different temperatures at 25˚C, 35˚C and 45˚C and the amount of uranium adsorbed was determined. Recyclability studies were performed using 0.1 M H_3PO_4 as desorbent. After each cycle, the adsorbent was filtered and equilibrated with 20 ml of 0.1 M H_3PO_4 for 30 min and the adsorbent was filtered, thoroughly washed with water and used for the consequent adsorption cycle.

2.5 Analytical Measurements

Fourier Transform Infra-red (FTIR) measurements were made with KBr pelts using Tensor 27 (Bruker, Germany) in the attenuated total reflectance (ATR) mode. FEI Quanta 200 machine was used for Scanning Electron Microscopy (SEM). XPS measurements were performed using PHI 5000 Versa Prob II,FEI Inc. spectrometer using nonmonochromatic Al Kα radiation (1486.6 eV). . XPSPEAK41 software with a Gaussian−Lorentzian line shape was used for the deconvolution of individual spectral peaks. A nonlinear Shirley background subtraction was applied for fitting each spectral region. The adsorbent was analyzed for the pore size distribution (PSD), specific surface area and pore volume by N_2-physisorption using Autosorb-1C instrument (Quantachrome, USA). Uranyl ions concentrations were determined by Inductive Coupled Plasma mass spectroscopy ICP-MS (Thermo, X-Series2). Calibration was carried out daily with freshly prepared uranium standards, before the sample analysis.

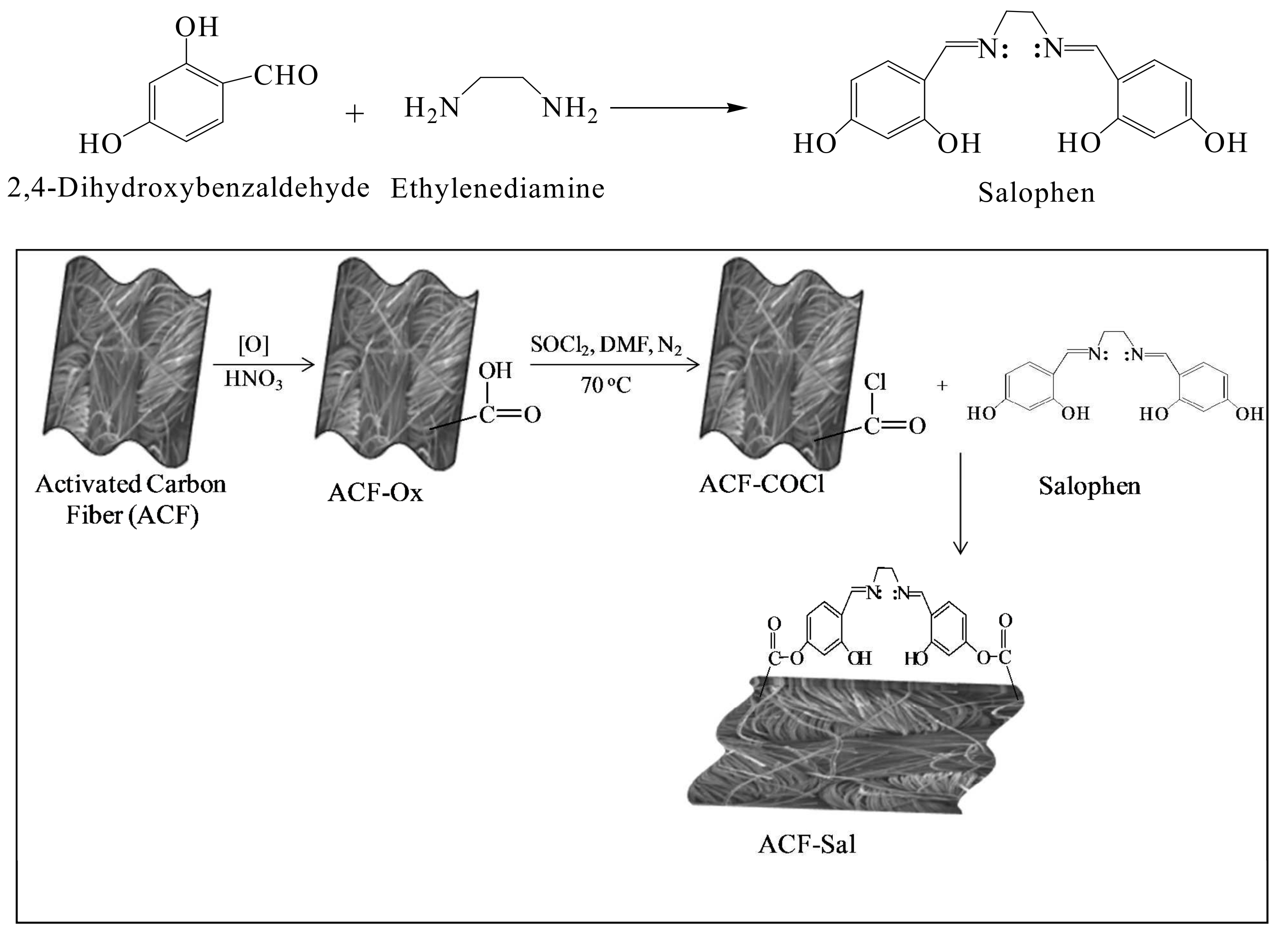

Scheme 1 Schematic representation of ACF Functionalization

3. Results and Discussion

3.1 Characterization of Adsorbent

3.1.1 SEM Analysis

SEM images of ACF, oxidized ACF, ACF-Sal are shown in Fig. 1 (a), (b), (c) respectively. ACF are composed of bundles of fibres with a diameter of about 10 µm. It is evident from the images that the surfaces of pristine ACF. ACF-OX and ACF-Sal are found to be smooth. The loading of uranium on ACF-Sal was confirmed from the Energy Dispersive X-ray analysis (EDAX) shown in Fig. 1d.

3.1.2 FTIR spectra

FTIR spectra from the ACFs show a broad peak at ~3445 cm^{-1} which is a characteristic of the O-H stretch of hydroxyl group (Fig. 2a) arising from the oscillation of carboxyl groups. The peaks at 2891 and 2920 cm^{-1} corresponds to $–CH_2$ and –CH symmetric stretch respectively. The C=C stretching vibration was found at 1632 cm^{-1}. Additional peak at 1720 cm^{-1} corresponding to C=O stretching was found after oxidation of ACF with nitric acid (ACF-OX) (Fig. 2b)[24]. In salophen anchored ACF (Fig.2c), the peaks at 1510 and 1620 cm^{-1} are attributed to the absorption of carbon-nitrogen double bond of the azomethine group[23]. Further additional peaks at 1210 cm^{-1} and 1116 cm^{-1} are due to the C-O and C-N stretching vibration respectively[21].

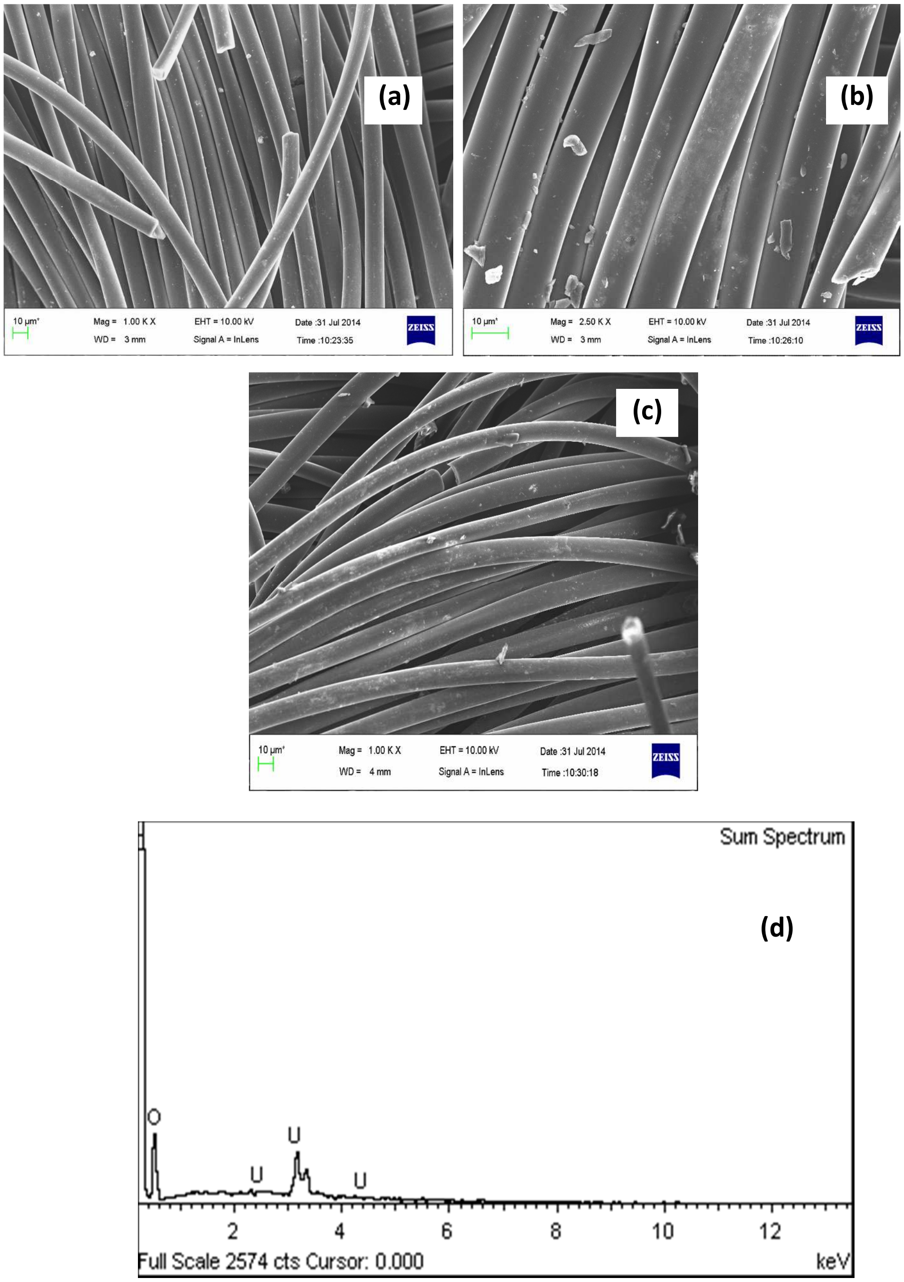

Fig.1 SEM images of (a) pristine ACF, (b) ACF-OX, (c) ACF-Sal, (d) ACF-Sal-U and (e) EDAX spectra of ACF-Sal-U

3.1.3 BET measurements

The specific surface area of the ACF, ACF-OX and ACF-Sal were obtained over the relative pressure range from 0.05 to 0.35 using the standard BET method. The total pore volume, mesopore and micropore volumes were caluculated using the instrument's software supplied by Quantachrome using Barrett–Joyner–Halenda (BJH) and density functional theory (DFT) methods. Table 1 summarizes the data for BET surface area and pore volumes of various ACFs. The large surface area and small pore size of these materials, lead to strong confinement of the adsorbed phase together with strong interactions with the surface. It is evident that the surface area of the ACFs increased from 1337 $m^2 g^{-1}$ to 1416.5 $m^2 g^{-1}$ upon oxidation with nitric acid and further grafting with Salophen ligand does not affect the surface area of the sorbent. During oxidation, the increased surface area could be attributed to the opening of pores. Marginal decrease in pore volumes of functionalized ACFs could be attributed to the blockage of inter-bundle galleries and intra-bundle interstitial channels by various functional groups.

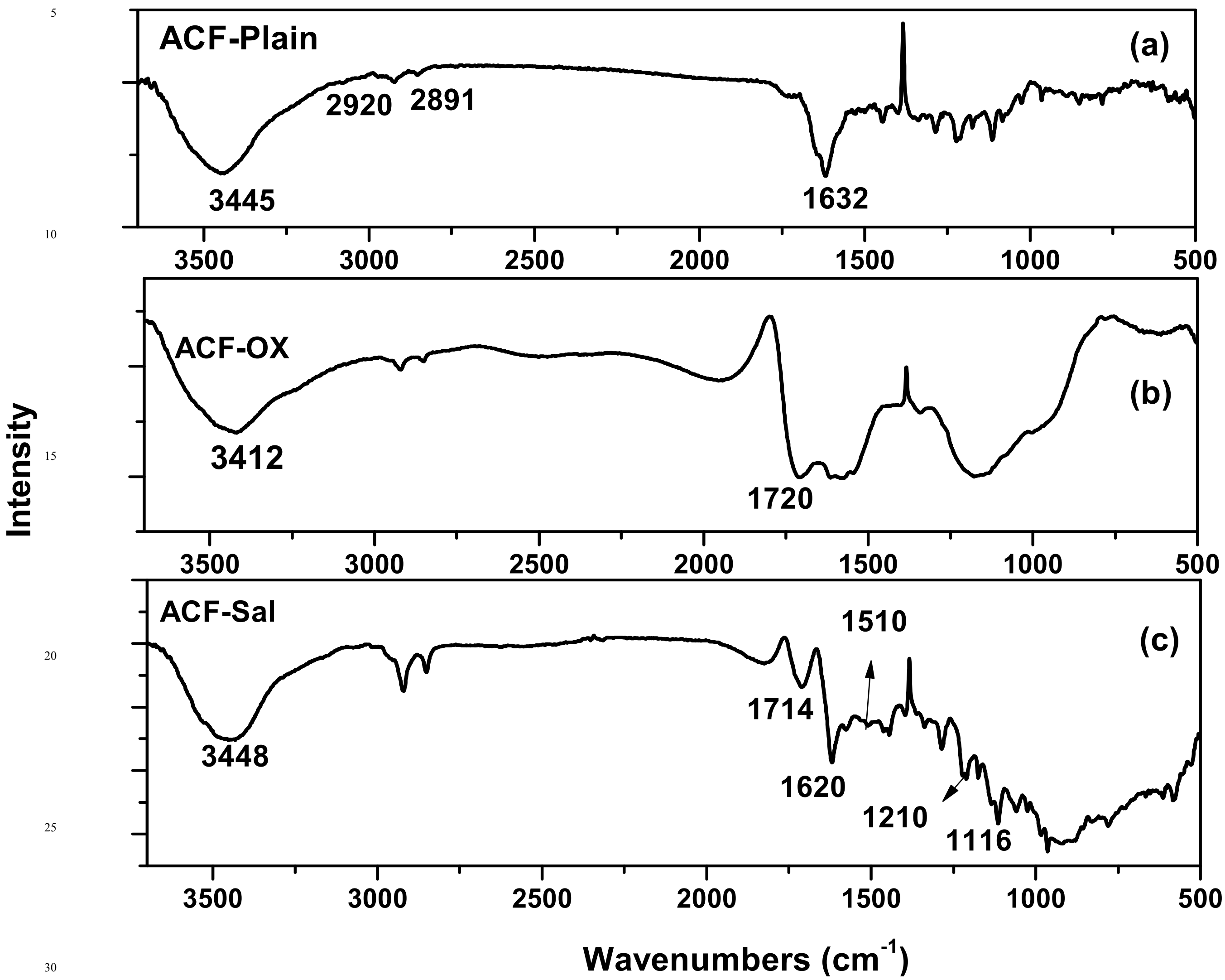

Fig. 2 FTIR Spectra of (a) Plain ACF (b) ACF-OX and (C) ACF-Sal

Table 1 Surface area and pore volumes of virgin and Functionalized ACF

Adsorbent	Surface Area (m^2/g)	Average Diameter (nm)	Total Pore Volume (cc/g)	Pore Volume (cc/g)	
				Meso	Micro
ACF	1337.0	2.10	0.7020	0.031	0.6320
ACF-OX	1416.5	0.95	0.6737	0.033	0.6407
ACF-Sal	1410.0	0.98	0.6800	0.032	0.6480

3.2 Effect of initial pH

Variation of initial pH in the range of 1 – 9 was examined using ACF, ACF-OX and ACF-Sal. Initial concentration of U(VI) was maintained at 100 mg/l. Efforts were made not to maintain the pH throughout the sorption experiments. The results obtained are shown in Fig. 3. It is evident from the figure that the sorption of U(VI) increased greatly from pH 4 to pH 6 and further increase in pH resulted in the decreased sorption. At pH ≤ 3, UO_2^{2+} is the predominant species of ions and sorption is found to be very low owing to the competition of H^+ ions for the active binding sites of the sorbent[9]. In the pH range of 5.5–7.5, the hydrolysis of uranyl ions occurs and various multinuclear hydroxyl complexes are prevalent including $UO_2(OH)^+$, $(UO_2)_2(OH)_2^{2+}$ and $(UO_2)_3(OH)_5^+$, [25]. Thus adsorption of U(VI) was found to be maximum at pH 6. At pH values greater than 7 anionic U(VI) species $(UO_2)_3(OH)_7^-$ was prevalent which resulted in low sorption capacity[26]. Further the amount of U(VI) increased from 18.56 mg/g to 35.2 mg/g after functionalization with salophen ligand. This can be explained by the complexation of U(VI) and Salophen ligand which are detailed in section 3.9.

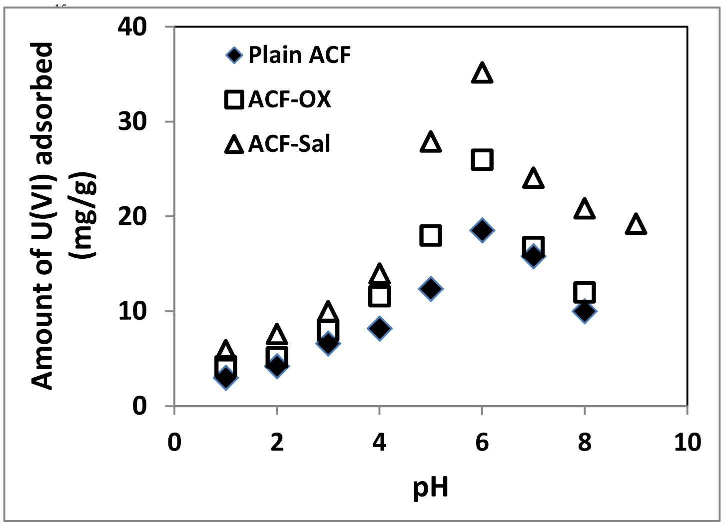

Fig 3. Effect of initial pH on ACF, ACF-OX and ACF-Sal with U(VI)

3.3 Effect of contact time

Sorption of U(VI) on ACF-Sal as a function of contact time was carried out at pH 6.0 ± 0.1. The results obtained are shown in Fig.4a. The sorption of U(VI) on ACF-Sal was shown to be rapid and a contact time of 3.5 h was enough to reach sorption equilibrium. Thus all the experiments were carried out at 4 h equilibration time. Kinetics of U(VI) adsorption onto ACF-Sal was modelled using Lagergren model[27] or pseudo first order, second order[28] and pseudo second order[29] shown in Eqns (2) – (4) respectively.

$$log(q_e - q_t) = log q_e - \frac{k_l}{2.303} t \qquad (2)$$

$$\frac{1}{q_e - q_t} = \frac{1}{q_e} + k_2 t \qquad (3)$$

$$\frac{t}{q_t} = \frac{1}{k_2' q_e^2} + \frac{t}{q_e} \qquad (4)$$

where k_L is the Lagergren rate constant of adsorption (min^{-1}); k_2 the second-order rate (g/mg/min) and k_2' the pseudo-second-order rate constant of adsorption (g/mg/min); qe and qt are the amounts of U(VI) ion sorbed (mg/g) at equilibrium and at time t, respectively. Plots of various models are depicted in Figs. 4b – 4d. The rate constants obtained for various kinetic models are given in Table 2. It is evident that among pseudo first order, second order and pseudo second order plot, pseudo second order plot of t/q_t *Vs t* Fig. 4(c) yielded straight line with correlation coefficients of > 0. 98. Thus it could be concluded that sorption of U(VI) with ACF-Sal followed pseudo second order kinetics. Since this model is based on the assumption that the rate-limiting step may be chemical sorption involving valency forces through sharing or exchange of electrons between sorbent and analyte, it is postulated that complex formation between the salophen ligand and U(VI) ions is the rate limiting step for the sorption of U(IV) onto ACF-Sal.

It is generally known that a typical solid/liquid sorption involves film diffusion or intraparticle diffusion as well. The probability of intraparticle diffusion could be modelled by Weber and Morris model[30] and this model relates the amount of the U(VI) adsorbed and the intraparticle rate constant (k_{int}) given by equation (5)

$$q_t = k_{int}\sqrt{t} + C \qquad (5)$$

The plot of q_t against $\sqrt{t}$ results in an intercept (Fig. 4e) . If the intraparticle diffusion is the sole rate determining step then the plot of q_t Vs √t should pass through origin with zero intercept. However, in the present scenario (Fig. 4e) is does not pass through origin. Hence we can conclude that intraparticle diffusion is not the sole rate determining step for the sorption of U(VI) on ACF-Sal. The value of intraparticle diffusion constant (k_{int}) of U(VI) was found to be 1.021 ($g\ mg^{-1}$) $(min^{0.5})^{-1}$ respectively.

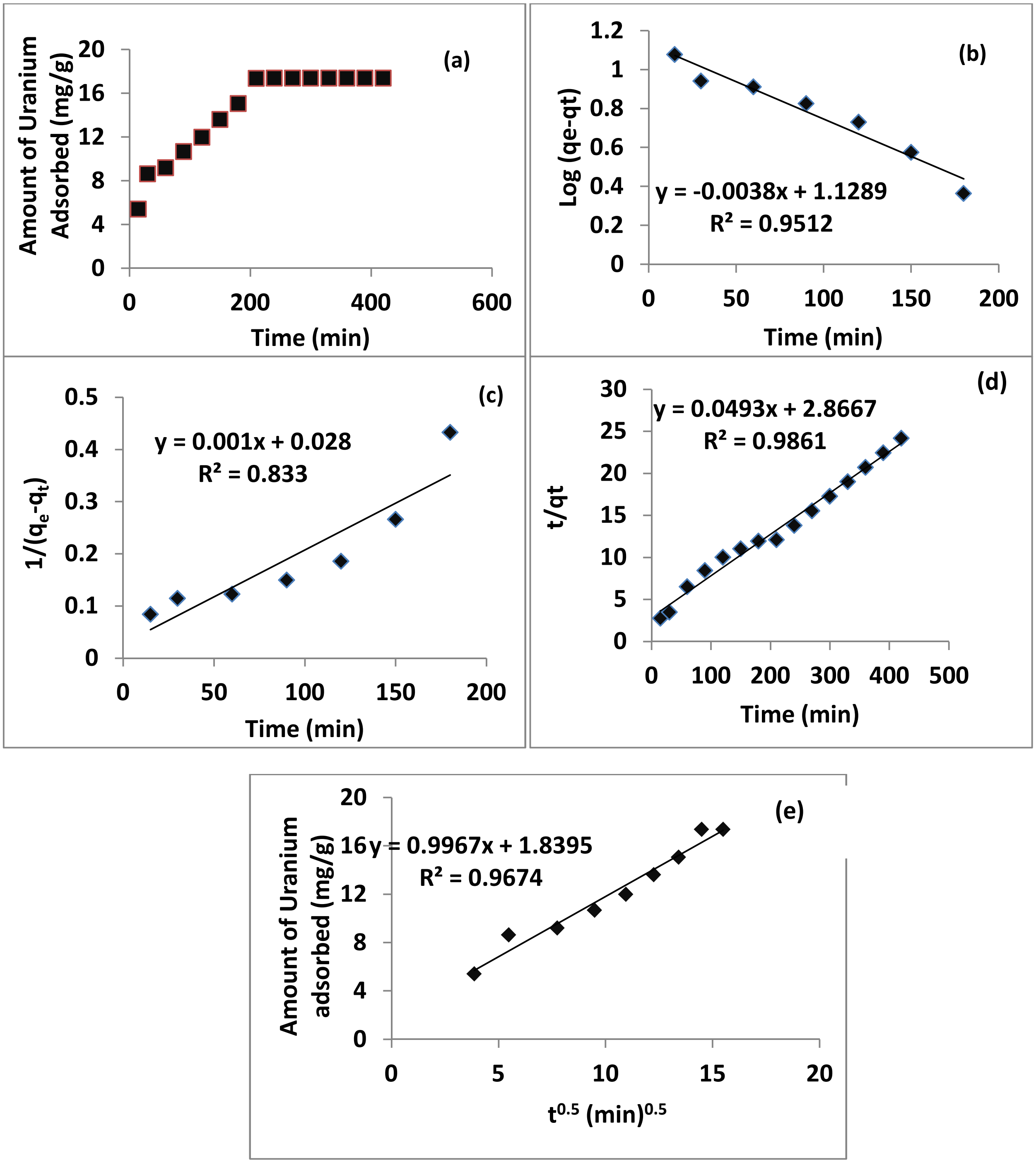

Fig. 4 a. Effect of Equilibration time b. Pseudo First order kinetic model c. Second Order kinetic model d. Pseudo Second Order kinetic model and e. Web-Morris model of ACF-Sal and Uranium system

Table 2 Kinetic Parameters of ACF-Sal and U(VI) systems

Pseudo First Order		Second Order		Pseudo Second Order	
K_l (min^{-1})	R^2	k_2 (mg/g/min)	R^2	k_2' (mg/g/min)	R^2
0.0069	0.951	0.001	0.833	0.0007	0.986

[a] Footnote text.

3.4 Sorption Isotherms

The U(VI) adsorption isotherms for ACF, ACF-OX, and ACF-Sal are presented in Fig. 5a. Adsorption data of U(VI)) over various functionalized ACFs were modelled using various isotherms. is The most commonly used Langmuir model describe the formation of homogeneous monolayer on the sorbent surface. The adsorption of U(VI) ions from the bulk to functionalized ACF surface could be expressed by Langmuir expression[31] as

$$q_e = \frac{q_m b C_e}{1 + b C_e} \qquad (6)$$

Where, q_e is the amount of U(VI) adsorbed (mg/g) at equilibrium and C_e is the equilibrium concentration (mg/L). The empirical constants q_m and b denote the maximum adsorption capacity and energy of adsorption, respectively, and were calculated from the slope and intercept of plot between $1/C_e$ and $1/q_e$ (Fig.5b). The constant 'b' is attributed to the affinity between the adsorbent and analyte in the given system. The values obtained for the various constants are given in Table 3. It is evident from Fig. 5a, that "S-isotherm" curve was obtained using ACF-Sal as adsorbent. The curve obtained is sigmoidal with a point of deflection. At low U(VI) concentrations, the adsorption is limited by the presence of the salophen ligand. After the complexation of U(VI) with the salophen ligand, normal adsorption occurs[32]. The point of inflection illustrates the concentration for which the other process of sorption overcomes the complexation. To further explain this behaviour, two site the data obtained was modelled by two site Langmuir isotherm[33] given by equation (7).

$$q_e = \frac{q'_m b' C_e}{1 + b' C_e} + \frac{q''_m b'' C_e}{1 + b'' C_e} \qquad (7)$$

The two-site Langmuir isotherms fit the adsorption data well when there are two types of adsorption sites with different binding energies on the adsorbents[33] q'_m (mg/g) and q''_m (mg/g), b_1 (L/mg) and b_2 (L/mg) in Eq. (7) are the maximum adsorption capacity and the affinity coefficients of sites 1 and 2 on the adsorbents, respectively. The total maximum adsorption capacity can be obtained by adding q'_m with q''_m. It is evident from the data that the maximum adsorption capacity of the three sorbents towards U(VI) were in the order of ACF-Sal > ACF-OX > ACF. It is evident that the sorption capacity of ACF-Sal from two site Langmuir model is 13.68 times higher than plain ACF. High sorption capacity of ACF-Sal towards U(VI) could be attributed to the formation of complex formation between salophen ligand and U(VI) ions. Adsorption capacity of ACF-Sal is significantly higher than the adsorption capacity of various carbon adsorbents, such as, plain oxidized MWCNT[26] (43.32 mg g^{-1}), Carboxymethyl cellulose grafted CNT[34] (112.0 mg g^{-1}), diglycolamide functionalized MWCNTs[35] (133.7 mg g^{-1}) , palm shell activated carbon[36](51.81 mg g^{-1}) and imine functionalized carbon spheres[37] (113 mg/g).

Further analysis of Langmuir model could be arrived based on a dimensionless equilibrium parameter called separation factor (R_L)[38].

$$R_L = \frac{1}{1 + bC_0} \qquad (8)$$

where C_0 is the initial concentration of U(VI) and 'b' is the Langmuir adsorption equilibrium constant (ml mg^{-1}). The value of R_L indicates the isotherm shapes to be favourable ($0<R_L<1$), unfavourable process (R_L <1), linear (R_L =1) or irreversible process (R_L =0). For an initial concentration of 100 mg L^{-1} U(VI) R_L values for ACF, ACF-OX and ACF-Sal were found to be 0.0115, 0.4016, and 0.7752 respectively. These values suggest the adsorption of uranyl ions by ACF and functionalized ACFs is a favourable process.

The heterogeneity of the system is described by Freundlich model and its linearized form is represented below[39]

$$\log q_e = \frac{1}{n}\log C_e + \log K_f \qquad (9)$$

Fig. 5d denotes the Freundlich plots of various sorbents. The n and K_f are the Freundlich parameters which represent the adsorption capacity and adsorption intensity respectively. For a good adsorbent the values of n ranged between 1 to 10. It is evident from Table 3 that the 'n' values ranged between 1.335 to 2.024 with a regression coefficient of 0.93 to 0.98 indicating the strong interaction of U(VI) ions with the adsorbent.

Table 3 Isotherm Parameters of ACF, ACF-OX and ACF-Sal with U(VI) systems

	Langmuir Model			Two Site Langmuir Model						Freundlich Model
Adsorbent	q_{max} (mg g^{-1})	b (L mg^{-1})	R^2	q_m' (mg g^{-1})	b' (L mg^{-1})	R^2	q_m'' (mg g^{-1})	b'' (L mg^{-1})	R^2	K_F (L g^{-1})
ACF	22.22	0.8640	0.96	-	-	-	-	-	-	2.673
ACF-OX	50.00	0.0149	0.94	-	-	-	-	-	-	2.138
ACF-Sal	142.86	0.0029	0.99	204.08	0.0023	1.00	101.01	0.0043	0.99	0.916

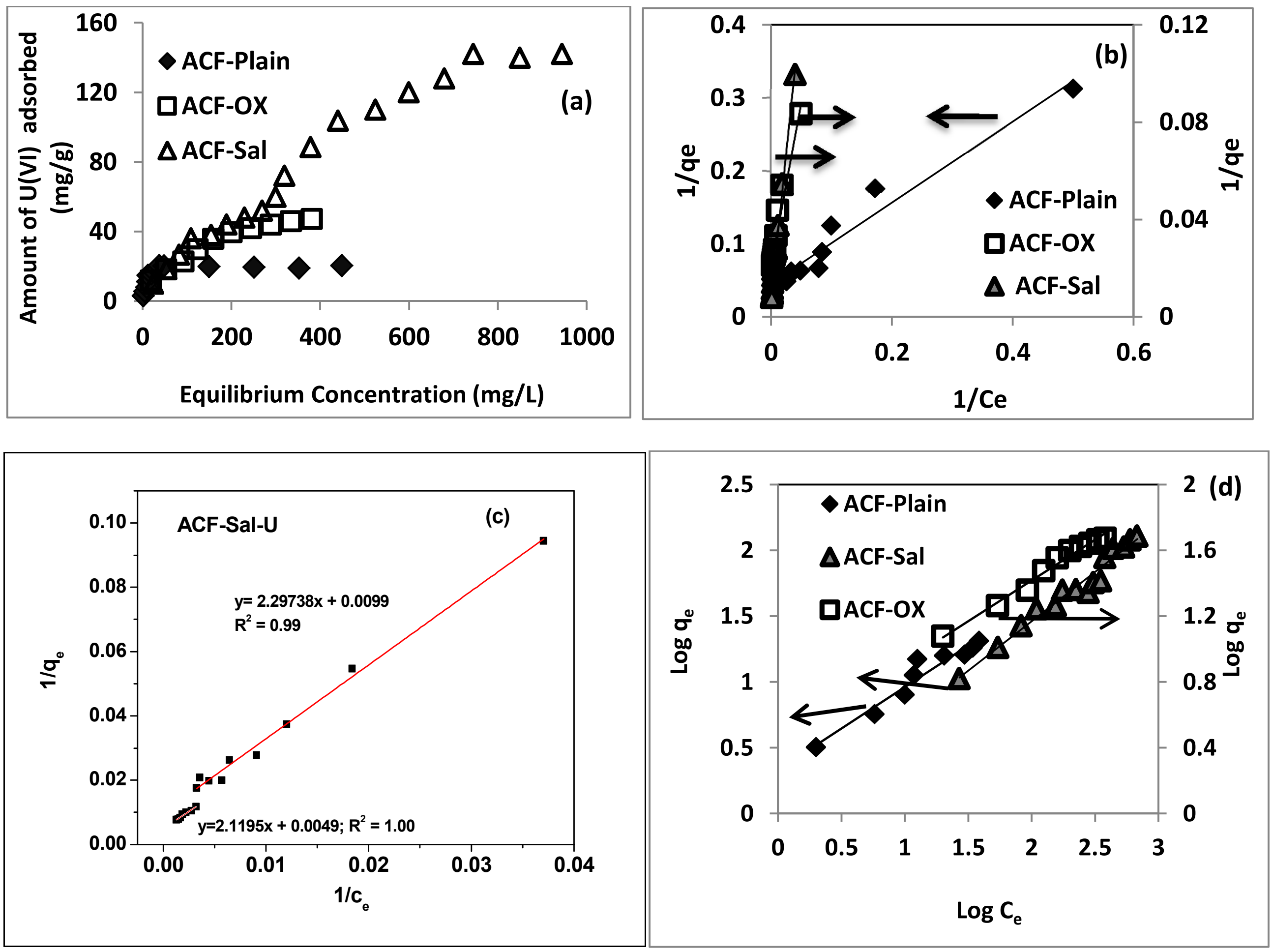

Fig. 5 (a) Equilibrium Isotherm, (b) Linearized Langmuir Plot and (C) Two site Langmuir Plot (d) Freundlich Plot

3.5 Thermodynamic Studies

The commonly used thermodynamic parameters such as ΔG°, ΔH° and ΔS° were calculated from the adsorption data[40]. Initially, *Kc,* the equilibrium constant was determined by eq. (10)

$$K_C = \frac{C_A}{C_e} \qquad (10)$$

where, C_A(g/L) is the concentration of solute in the aqueous phase and C_e is the equilibrium concentration (g/l). ΔG° was calculated using the following equation:

$$\Delta G^\circ = -RT \ln Kc \qquad (11)$$

where R is the gas constant, T is the temperature in Kelvin. Using Van't Hoff equation (12) the value of ΔS and ΔH was determined:

$$\log Kc = \frac{\Delta S^\circ}{2.303} - \frac{\Delta H^\circ}{2.303RT} \qquad (12)$$

Based on the above-calculated data, a linear plot of $\ln K_c$ vs. 1/T was drawn for U(VI) and ACF-Sal system (Fig.6). Using these plots, ΔS° and ΔH° were determined from the intercept and slope, respectively. The data obtained are presented in Table 4. The negative free energy values indicate the spontaneity and feasibility of the process, while the positive ΔH° values indicate the endothermic nature of the process. Further, positive values of the entropy (Δ*S*°) of adsorption could be attributed to metal ion dehydration due to surface sorption on ACF-Sal.

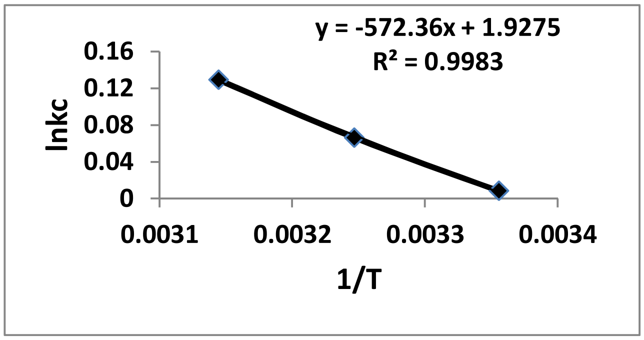

Fig.6 Thermodynamic studies of ACF-Sal and U(VI) systems

Table 4. Thermodynamic Parameters

T (K)	Ce (g/l)	Kc	ΔG (KJ/mol)	ΔS (J/mol)	ΔH [kJ/(mol/K)]
298	0.2476	1.0192	-0.0472		
308	0.2309	1.1649	-0.3909	4.439	10.96
318	0.2131	1.3463	-0.7863		

3.6 Recyclability Studies

Uranium desorption studies were conducted after sorption of U(VI) using ACF-Sal as sorbent. The conditions for adsorption were maintained as prescribed in Sec 2.4. After adsorption of U(VI) ions, the sorbents were filtered and washed with water and and 0.1 M H_3PO_4 was used as desorbent. The sorption desorption cycle was repeated for 5 cycles. The amount of U(VI) adsorbed by ACF-Sal for five consecutive sorption-desorption cycle are depicted in Fig. 7. It is evident from the figure that around 20 and 40% decrease in U(VI) uptake was observed at the end of 3rd and 5th cycle respectively. A similar result has been reported using ordered mesoporous carbon as adsorbent[11].

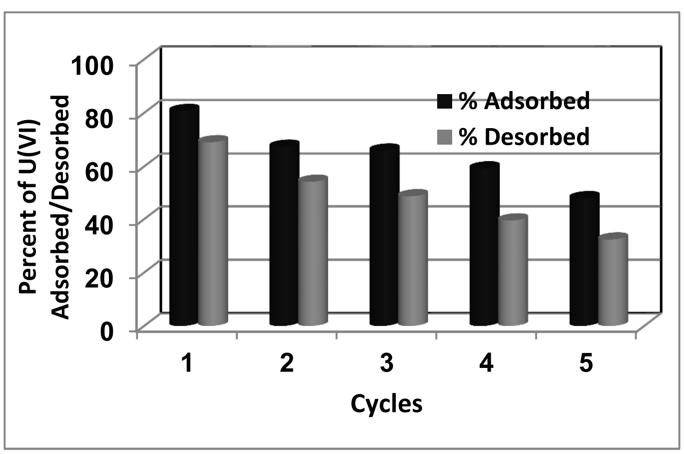

Fig.7 Recyclability Studies

3.7 Effect of competing ions

Uranium sorption by ACF-Sal in the presence of other cations and anions was studied. Initially, 100 ppm of U(VI) was spiked with known concentrations of anions/cations and pH was adjusted to 6 and equilibrated for 3h. After equilibration the solution was filtered and the amount of U(VI) adsorbed was analyzed using ICPMS instrument. The effect of these ions on the sorption process may be represented by the ratio of adsorption capacity in the presence of interfering ion (q_{mix}) and without interfering ion (q_0), as shown below[41] :

$q_{mix}/q_0 > 1$ increased adsorption in the presence of other interfering ions

$q_{mix}/q_0 = 1$ adsorption is not influenced in the presence of other interfering ions

$q_{mix}/q_0 < 1$ adsorption is suppressed in the presence of other interfering ions

The effect of cations and anions on the sorption capacity of ACF-Sal is detailed in Table 5a and 5b respectively.

The order of interfering effect of the various cations tested is $Cd^{2+} > Ni^{2+} > Pb^{2+} > Cu^{2+} > Ca^{2+} >>.> Mn^{2+}$. Increased interfering effect was observed for Cd^{2+}, Ni^{2+} and Pb^{2+} ions. This could be attributed to their complexation with salophen ligand and non availability of these complexing sites for U(VI) sorption. Among the various anions tested it is interesting to observe that a slight increase on sorption of U(VI) ions is observed in the presence of phosphate ions. Coordination around uranium is pentagonal bipyramidal with the four donor atoms of the salophen ligand occupying the equatorial plane and the uranyl oxygen atoms in the axial positions. The fifth equatorial site of the metal remains available for coordination by an additional group, either an anion or a neutral molecule. Due to the high affinity of UO_2^{2+} to phosphate anions[42], the stability constants of Sal−UO_2−$H_2PO_4^-$ is larger than other anions (Cl^-, SO_4^{2-}, NO_3^-) tested and the data is furnished in Table 6. This explains for the increased uptake of U(VI) by ACF-Sal in the presence of phosphate ions. Further it should be noted that when desorption studies were conducted with (0.1M H_3PO_4) around 85% of the U(VI) was found to be desorbed (Sec 3.6). This is probably because the acidity of the desorbing solution is around pH 1 and at this acidity, U(VI) salophen complex is unstable and Uranyl-phosphate complexation takes place which results in leaching of U(VI) from the sorbent surface.

Table 5a. Effect of competing cations on sorption of U(VI) by ACF-Sal

Cations	q_{mix}/q_o	
	100 mg/l	200 mg/l
Ni^{2+}	0.91	0.89
Cd^{2+}	0.82	0.76
Ca^{2+}	0.97	0.94
Pb^{2+}	0.90	0.86
Cu^{2+}	0.99	0.92
Mn^{2+}	1.00	1.00

Table 5b Effect of competing anions on sorption of U(VI) by ACF-Sal

Anions (0.1 M)	q_{mix}/q_o
Sulphate	**0.97**
Chloride	**0.93**
Nitrate	**1.00**
Phosphate	**1.10**

Table 6 The Experimental Stability Constants (K_{ass}) for the Uranyl Salophene (US1) Complexation with Anions[a]

Complex	K_{ass} [M^{-1}]
$Sal–UO_2–Cl^-$	4.5×10^2
$Sal–UO_2–NO_2^-$	3.1×10^2
$Sal–UO_2–HSO_4^-$	5.0×10^1
$Sal–UO_2–H_2PO_4^-$	1.1×10^4

[a] Adapted from ref Stauthammer, W. Ph.D. Thesis, University of Twente, The Netherlands, 1994.

3.8 XPS evaluation

In order to study the sorption of U(VI) onto ACF, ACF-OX and ACF-Sal, XPS spectra were recorded after U(VI) loading. The O 1s, C 1s, and U 4f of the sorbents were demonstrated in Fig.8. In the survey spectra (Fig. 8), the characteristics doublet peaks of U $4f_{5/2}$ and U $4f_{7/2}$ were observed for all the loaded sorbents. The binding energies of the various peaks and the splitting values of Uranium peaks are depicted in Table 7. The peak positions of U(VI) adsorbed on ACF-Sal shifted to relative high binding energies as compared to those of U(VI) adsorbed onto ACF and ACF-OX, which could be attributed to the stronger interaction of U(VI) with ACF-Sal compared to ACF and ACF-OX. A similar observation was observed by other researchers on uranyl sorption onto to chitosan modified CNTs[43]. Further comparing the the splitting values of $4f_{5/2}$ and $4f_{7/2}$ peaks of U(VI) ions onto ACF, ACF-OX and ACF-Sal, an increasing trend is observed which could be attributed to stronger interaction of U(VI) with salophen ligand.

In order to further probe the mechanism of U(VI) sorption on to ACF-Sal at molecular level, the XPS spectra of survey and high resolution scans for O 1s, N 1s, and U 4f on ACF-Sal were recorded. The O 1s, N 1s, and U 4f of the ACF-sal before and after U(VI) sorption (denoted as ACF-Sal-U) were demonstrated in Fig. 9. The peak fitting results of the U 4f, O 1s, N 1s before and after U(VI) sorption on ACF-Sal are listed in Table 8. From Fig. 9e, the U $4f_{7/2}$ spectrum was resolved into two peaks: the peak at 379.5 eV corresponded to the free uranyl adsorbed on ACF-Sal, and the peak at 381.08 eV was attributed to covalent bond of azomethine N-U(VI)[44]. From Fig.9b, the O 1s spectra could be resolved into three main peaks occurring at 530.54, 531.94 and 532.77 eV , respectively, corresponding to O=C, C-O-C and H-O-H bonds[45]. Thus, XPS studies have been have been used to study the efficient anchoring of Salophen ligand onto CNT back bone[46]. After U(VI) sorption (Fig 9d) four different peaks occurred at 529.47, 529.97, 530.53, 531.85 eV. Additional peak after U(VI) sorption could be attributed to the presence of U=O bond[46,47]. Further the shift in the binding energies of O 1s before and after U(VI) loading indicated that indicated that U(VI) sorption onto ACF-Sal occurred by the complexation of oxygen-containing functional groups. Calculating the content of elements on surface of ACFs by area of each element, we can find that the weight content of N is about 3.2%, indicating the presence of Schiff-base groups. Figures 9a and 9c shows the core level N 1s of ACF-Sal before and after U(VI) sorption respectively. The N 1s spectrum was resolved into two individual component peaks at 395.5 and 402.0 eV[48]. After uranyl sorption the peaks shifted to higher binding energies due to the charge transfers occurring from Nitrogen containing salophen ligand to U(VI) ions.

Thus the results from XPS studies suggests that the salophen ligand is efficiently anchored onto to ACF surface and U(VI) complexation occurred with the tetradentate N(2)O(2) donors derived from the phenolic oxygen and azomethine nitrogen of the saplohen ligand

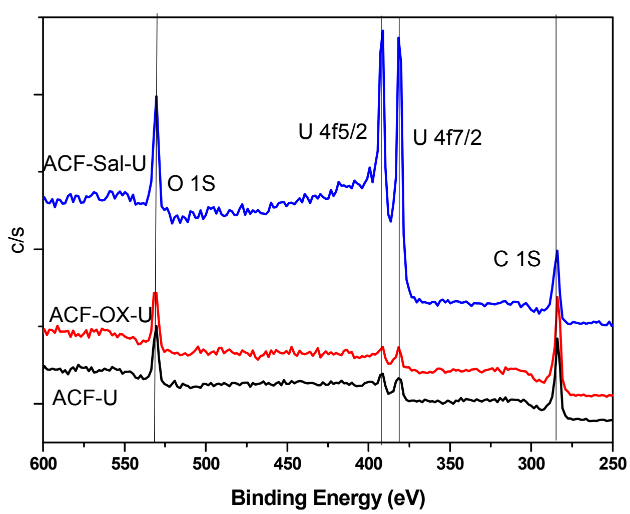

Fig.8 Uranium loaded XPS wide scans of ACF, ACF-OX and ACF-Sal

Cite this: DOI: 10.1039/c0xx00000x

www.rsc.org/xxxxxx

ARTICLE TYPE

Table7 Binding energies(eV) of ACF, ACF-OX and ACF-Sal after Uranium adsorption

Type	C 1s	O 1s	N 1s	U 4f5/2	U 4f7/2	Splitting values
ACF-U	284.35	530.80	-	390.87	381.00	9.87
ACF-OX-U	284.48	530.43	-	391.57	381.25	10.32
ACF-Sal-U	285.30	531.35	398.53	391.67	381.30	10.37

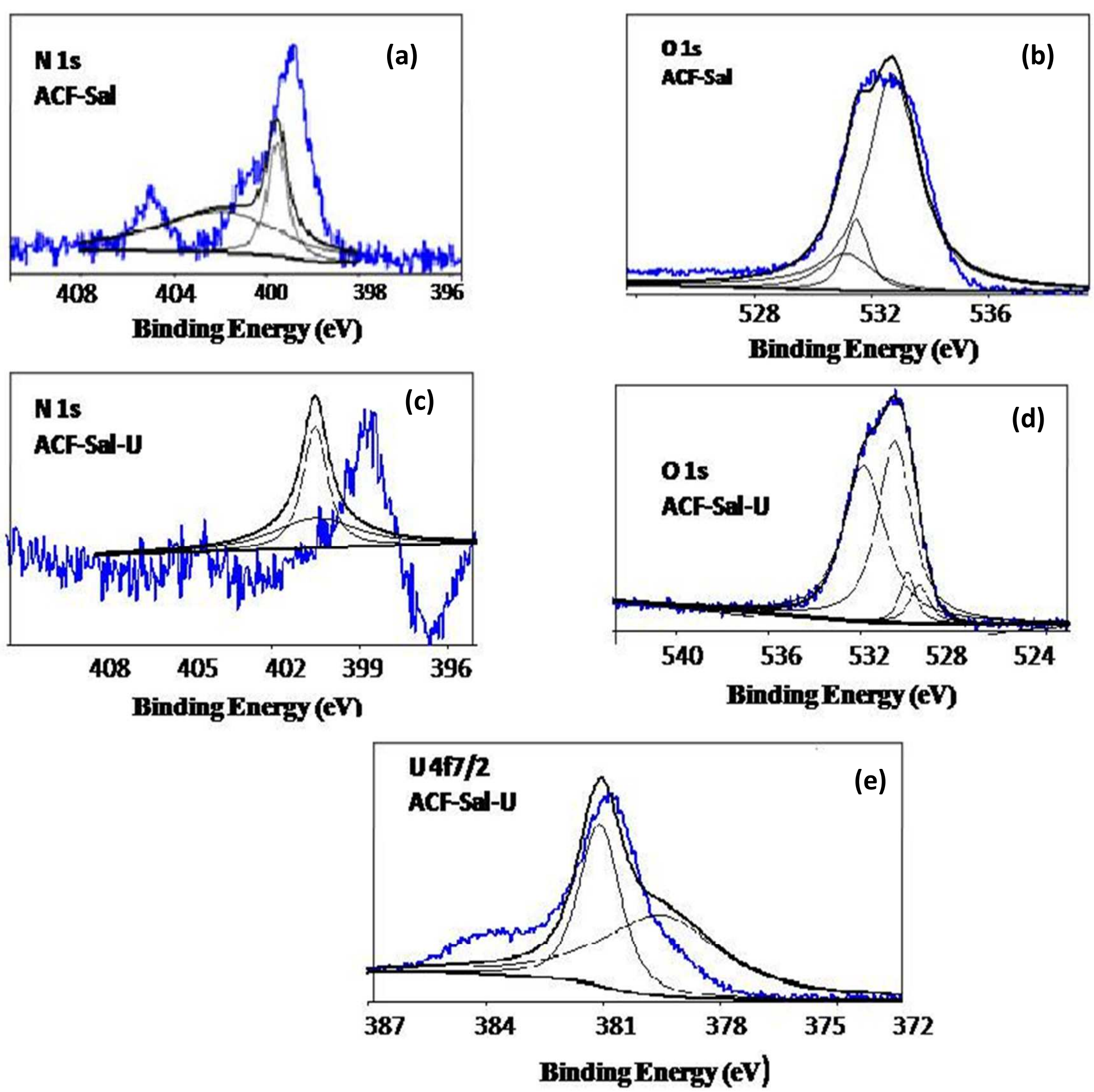

Fig.9 Curve fitted high resolution XPS scans of ACF-Sal for (a) O 1s, (b) N 1s before U(VI) loading and (c) O 1s, (d) N 1s and U 4f (e) after U(VI) loading

Journal Name

Cite this: DOI: 10.1039/c0xx00000x

www.rsc.org/xxxxxx

ARTICLE TYPE

Table 8 Core level binding energies of ACF-Sal and U(VI) loaded ACF-Sal systems

Core levels	ACF-Sal			ACF-Sal-U		
	Binding Energy (eV)	FWHW (eV)	Area	Binding Energy (eV)	FWHW (eV)	Area
N 1s	395.5	1.00	143.38	400.50	3.520	82.12
	402.0	6.386	336.99	406.09	0.592	0.59
O 1s	530.54	1.69	2326.78	531.85	2.230	2154.16
	531.94	1.37	982.99	530.53	1.766	2002.55
	532.77	1.51	186.71	529.47	1.000	243.86
	-	-	-	529.97	0.810	252.97
U 4f7/2	-	-	-	379.5	3.543	1148.07
	-	-	-	381.08	1.263	735.34

3.9 Mechanism of Interaction

Adsorption of U(VI) onto ACF and ACF-OX might be attributed to both ion exchange and electron donating acceptor complexation reactions at the surface sites. At pH 6.0 where maximum removal of U(VI) is observed (Fig.3), 95% of the uranyl ions exists as$(UO_2)_3(OH)_5^+$ species and less from UO_2^{2+} [49]. It is well known that pH 6.0 carboxyl groups are deprotonated and there exists a strong complexation between the hydrolyzed uranyl ions $[(UO_2)_3(OH)_5^+]$ and carboxyl groups. The FTIR spectra of ACF, ACF-OX and ACF-Sal before and after loading with U(VI) is shown in Fig. 10. It is evident from the spectra that after U(VI) loading in ACF (Fig.10a), the hydroxyl peak shifts from 3437 cm^{-1} to 3418 cm^{-1} which confirms the involvement of OH group and further a sharp peak at 920 cm^{-1} confirms the υ_3 band of uranyl ions [50,51]. In U(VI) loaded ACF-OX, shifting of the carbonyl stretching peak from 1721 to 1715cm^{-1} is observed. Additionally, a uranyl band appears at 906 cm^{-1} characteristic of the υ_3 band of uranyl ions described earlier. Also, the U(VI) removal might be attributed to the electron donating acceptor (EDA) complexation between the de-localized π-electron of graphene layers of ACF and $(UO_2)_3(OH)_5^+$ by dispersive forces[52]. The main mechanism governing the sorption of U(VI) onto ACF-Sal is the complexation reaction occurring between the salophen ligand and the uranyl ions. After complexation with U(VI) (Fig. 10c), the environment of C=N changes and a shift from 1620 to 1615 cm^{-1} is observed. Further the stretching vibrations of –C-O and C-N exhibited a slight upfield shift to 1220 cm^{-1} and 1124 cm^{-1} respectively owing to the complexation[21]. As observed in ACF, ACF-OX, in U(VI) loaded ACF-Sal, υ_3 uranyl band appeared around 890 cm^{-1}. The shifting of the frequencies of the uranyl band depends on the ligands present in the equatorial plane. Generally, the asymmetrical uranyl stretching frequency ranges from 885 – 899 cm^{-1} for uranyl complexes with schiff's base [53 - 58]. This further confirms the complexation between U(VI) and salophen ligand.

From the above discussions from FTIR and XPS studies, a mechanism has been suggested in scheme 2 depicting the complexation of uranium and salophen ligand.

Cite this: DOI: 10.1039/c0xx00000x
www.rsc.org/xxxxxx

ARTICLE TYPE

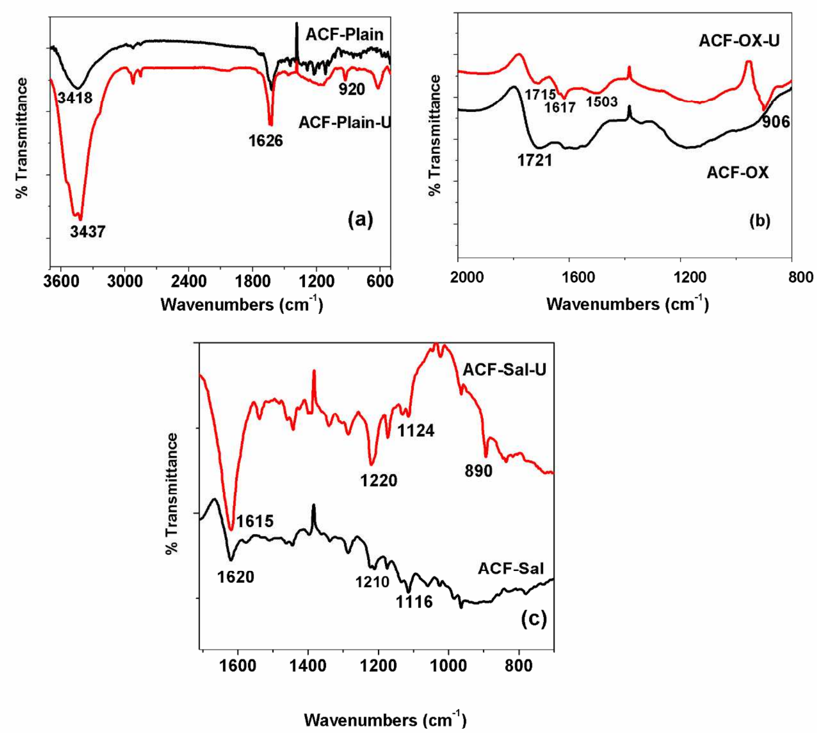

Fig.10 FTIR spectra of (a) ACF (b) ACF-OX and (c)ACF-Sal before and after loading Uranyl ions

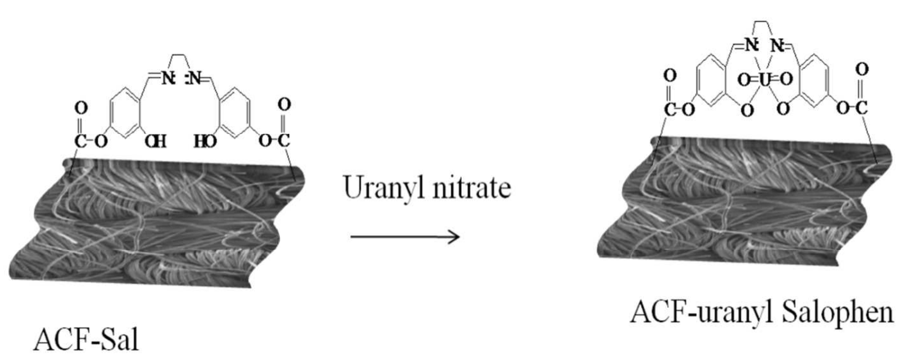

Scheme 2. Schematic representation of complexation of U(VI) with ACF-Salophen

Cite this: DOI: 10.1039/c0xx00000x

www.rsc.org/xxxxxx

ARTICLE TYPE

4. Conclusions

Functionalized activated carbon fibres were prepared by oxidation and grafting Salophen ligand. The prepared sorbent materials were characterized by various spectral techniques. Kinetics followed a pseudo second order model and removal of U(VI) was found to be maximum at pH 6. The experimental data obtained were analyzed by various isotherms including Langmuir, and Freundlich and the adsorption capacity of the functionalized ACFs were in the order of ACF-Sal > ACF-OX > ACF. The observed high capacity (142.8 mg/g for ACF-Sal by Langmuir and 305.09 mg/g by two site Langmuir model) could be attributed to the bonding of U(VI) and the salophen ligand. Effect of other commonly occurring cations and anions on the sorption U(VI) by ACF-Sal was studied. Thermodynamic studies revealed the spontaneity of the reaction and the sorbent could be recycled for 5 sorption-desorption cycles. From the FTIR and XPS studies a suitable mechanism for sorption has also been proposed.

Notes and references

[a] *Centre for Environmental Science and Engineering, Indian Institute of Technology Kanpur, Kanpur, U.P. 208016, India*
[b] *Department of Chemistry, Banasthali Vidyapith, Rajasthan 304022, India*
[c] *Bhabha Atomic Research Centre, Trombay, Mumbai, India*
**Author for Correspondence*
Email: nalini@iitk.ac.in Tel: +91915122596360

Acknowledgements Authors thank the funding received from Board of Research in Nuclear Sciences, Department of Atomic Energy, Mumbai, India (Ref. No. 2013/36/57-BRNS/2482) to carry out this work

1. G. M. Naja and B. Volesky, Toxicity and sources of Pb, Cd, Hg, Cr, As and radionuclides in the environment, CRC Press, Taylor & Francis Group, USA, 2009, 16.
2. WHO, Guidelines for Drinking Water Quality, Geneva, 2nd edn, 1998, 283.
3. A.Kilincarslan and S. Akyil, *J. Radioanal. Nucl. Chem.*, 2005, **264**, 541.
4. P. D. Bhalara, D. Punetha and K. Balasubramanian, *J. Environ. Chem. Eng.*, 2014*,* **2,** 1621.
5. P. Swain, C. Mallika, R. Srinivasan, U. K. Mudali and R. Natarajan, *J. Radioanal. Nucl. Chem.,* 2013, **298**, 781.
6. A. M. A. Morsy and A. E. M. Hussein, *J. Radioanal. Nucl. Chem.,* 2011, **288**, 341.
7. M. Caccin, F. Giacobbo, M. Da Ros, L. Besozzi and M. Mariani, *J. Radioanal. Nucl. Chem.,* 2013, **297**, 9.
8. Y. Sun, S. Yang, G. Sheng, Z. Gua and X. Wang, *J. Environ. Radioact.,*2012, **105,** 40.
9. Schierz and H. Zanker, *Environ. Pollut.*, 2009, **157**, 1088.
10. D. D Shao, Z. Q Jiang, X. K. Wang, J. X. Li and Y. D. Meng, *J. Phys. Chem.*, 2009, **113**, 860.
11. B-W Nie, Z-B Zhang, Xiao-hong Cao, Yun-hai Liu and Ping Liang, *J. Radioanal. Nucl. Chem.*, 2012, **295**, 663.
12. V. Gaur, A. Sharma and N. Verma, *Chem. Eng. Process.,* 2006, **45**, 1–13.
13. B.M. Babić, S.K. Milonjić, M.J. Polovina, S. Čupić, B.V.Kaludjerović, *Carbon*, 2002, **40** 1109..
14. R. Leyva-Ramos, M. S. Berber-Mendoza, J. Salazar-Rabago, R. M. Guerrero-Coronado and J. Mendoza-Barron, *Adsorption*, 2011, **17**, 515.
15. J.R. Rangel-Mendez and M. Streat, *Water Res.*, 2002, **36,** 1244.
16. M. A. Alvarez-Merino, V. Lopez-Ramon and C. Moreno-Castilla, *J. Colloid Interface Sci.*, 2005, **288**, 335.
17. M. S. Berber-Mendoza, R. Leyva-Ramos, F. J. Cerino-Cordoba, J. Mendoza-Barron, H. J. Amezquita Garcia and J. V. Flores-Cano, *Water, Air, Soil Pollut.,* 2013, **224**, 1604.
18. X. Zhou**,** H. Yi, X. Tang, H. Deng and H. Liu, Chem. Eng. J., 2012, **200-202**, 399
19. M. Bikshapathi**,** S. Mandal, G. N. Mathur**,** A. Sharma and N. Verma, Ind. Eng. Chem. Res., 2011, **50**, 13092-13104.
20. C.-H. Jung, H.-Y. Lee, J.-K. Moon, H.-J. Won and Y.-G. Shul, *J. Radioanal. Nucl. Chem.*, 2011, **287**, 833.
21. M. Wu, L. Liao, M. Zhao, Y. Lin, X. Xiao, C. Nie Anal. Chim acta., 2012, **729**, 80.
22. J. L. Sessler, P. J. Melfi and G. D. Pantos, *Coordin. Chem. Rev*., 2006, **250,** 816.
23. M. Salavati-Niasari and M. Bazarganipour, *Appl. Surf. Sci.*, 2008, **255**, 2963-2970.
24. C.-C. Huang and Y.-J. Su, J. Hazard. Mater., 2010, **175**, 477.
25. G. Wang, J. Liu, X. Wang, Z. Xie and N. Deng, *J. Hazard. Mater*., 2009, **168,** 1053–1058.
26. M.Wang, J. Qiu, X. Tao, C. Wu, W. Cui, Q. Liu, S. Lu, *J. Radioanal. Nucl. Chem*., 2011, **288**, 895
27. S. Lagergren*, Handlingar*, 1898, **24**, 1–39.
28. Y. S. Ho, D. A. J. Wase and C. F. Forster, *Environ. Tech*. 1996, **17**, 71.
29. Y.S. Ho and G. McKay, *Advances in Adsorption Separation Science and Technology*, South China University of Technology Press, Guangzhou, 1997, 257-263.
30. W. J. Weber and J. C. Morris, *J. Sanit. Eng. Div. Am. Soc. Civ. Eng*., 1963, **89**, 31.
31. Langmuir, *J. Am. Chem. Soc.*,1918, **40,** 1361.
32. Sposito, G., 1982. On the use of the Langmuir equation in the interpretation of ‘‘adsorption’’ phenomena: II. The ‘‘twosurface’’ Langmuir equation. Soil Sci. Soc. Am. J. 46, 1147–1152.
33. Y. Jin, F. Liu, M. Tong, Y. Hou, *J. Hazard. Mater,* 2012, **227** 461.
34. D. Shao, Z. Jiang, X. Wang, J. Li, Y. Meng, *J. Phys. Chem. B* 2009, **113**, 860.
35. A. K. S. Deb, P. Ilaiyaraja, D. Ponraju and B. Venkatraman*, J. Radioanal. Nucl. Chem.*, 2012, **291**, 877.
36. Z.-J. Yi, J. Yao, J.-S. Xu**,** M.-S. Chen, W. Li, H.-L. Chen and F. Wang, J. Radioanal. Nucl. Chem., 2014, **301**, 695.
37. P. S. Dubey, D. A. Dwivedi, M. Sillanpaa, Y.-N. Kwon and C. Lee**,** RSC Adv., 2014, **4**, 46114.
38. N. Sankararamakrishnan, A. Dixit, L. Iyengar and R.sanghi, *Bioresour. Technol.,* 2006, **97**, 2377**.**
39. H. M. F. Freundlich, *J. Phys. Chem.*, 1906, **57**, 385.
40. P. Perrot, A to Z of Thermodynamics, Oxford University Press, New York, 1998.
41. F. V. Pereira, L. V. A. Gurgel and L. F. Gil, *J. Hazard. Mater.*, 2010, **176**, 856 .

42. M. Merdivan, M. B. Buchmeister and G. Bonn, *Anal. Chim. Acta*, 1999, **402**, 91.
43. J.-H. Chen, D.-Q. Lu, B. Chen and P.-K. Ouyang, *J. Radioanal. Nucl. Chem.*, 2013, **295**, 2233.
44. W.Song, M.Liu, R.Hu, X.Tan, J.Li, *J.Chem.Eng.,* 2014, **246**. 268.
45. M. Salavati-Niasari**,** F. Davar and M. Bazarganipour, *Dalton Trans*., 2010, **39**, 7330.
46. S.Vanden Berghe, F. Miserque, T. Gouder, B. Gaudreau and M. Verwerft, *J. Nucl. Mater*, 2001, **294**, 168.
47. S. Chen, J. Hong, H. Yang and J. Yang, *J. Environ. Radioact.*, 2013, **126**, 253 .
48. R.J.J. Jansen and H. van Bekkum, Carbon, 1995, **33**, 1021.
49. E. Guibal, C. Roulph and P. Le Cloirec, *Water Res.*, 1992, **26**, 1139.
50. R.L. Frost, *Spectrosc. Acta., A: Mol. Biomol. Spectrosc*. 2006, **64**, 308
51. M. Tsezos, B. Volesky*, Biotechnol. Bioeng*. 1982, **24**, 385
52. S.M. Yakout, S. S. Metwally and T. El-Zakla, *Appl. Surf. Sci*, 2013, **280**, 745.
53. K. Mizuoka, S. –Y. Kim, M. Hasegawa, T. Hoshi, G. Uchiyama and Y. Ikeda, *Inorg. Chem*., 2003, **42**, 1031;
54. K. Mizuoka, S. Tsushima, M.Hasegawa, T. Hoshi and Y. Ikeda, *Inorg. Chem*., 2005, **44**, 6211;
55. K.Mizuoka and Y. Ikeda, *Radiochim. Acta*, 2004, **92**, 631
56. L. Cattalini, S. Degetto, M. Vidali and P. A. Vigato, *Inorg. Chim. Acta,* 1972, **6** , 173.
57. E. M. Nour, A. A. Taha and I. S. Alnaimi, *Inorg. Chim. Acta*, 1988, **141**, 139.